OBSERVATIONS OF 1000 km s^{-1} DOPPLER SHIFTS IN 10^7 K SOLAR FLARE SUPRA-ARCADE

D. E. INNES[1], D. E. McKENZIE[2] and TONGJIANG WANG[1]
[1]*Max-Planck-Institut für Aeronomie, Max-Planck-Str. 2, 37191 Katlenburg-Lindau, Germany*
(e-mail: innes@linmpi.mpg.de)
[2]*Department of Physics, Montana State University, P.O. Box 173840, Bozeman, Montana 59717-3840, U.S.A.*

(Received 13 March 2003; accepted 18 July 2003)

Abstract. An X1.5 flare on the west limb of the Sun on 21 April 2002 developed a large supra-arcade about 30 min after flare onset. The growth of the supra-arcade can be followed in both TRACE 195 Å images and SUMER spectra. Its growth seems to be associated with dark (in TRACE images), sunward moving channels that descend onto the arcade from above. SUMER recorded Doppler shifts of 800–1000 km s^{-1} in Fe XXI 1354 Å from positions where this sunward flow interacts with the arcade tops. We describe the observations, focusing on the relationship of the high Fe XXI line shifts to the sunward moving dark flows.

1. Introduction

An eruptive flare that occurred on 21 April 2002 on the west limb of the Sun developed a large supra-arcade fan of hot plasma rays (Gallagher *et al.*, 2002), against which dark flows (in TRACE extreme ultraviolet (EUV) images) were seen falling towards the Sun. The event is unique because it the only one of its type for which simultaneous high-cadence images and spectra of the arcade and the sunward flows are available. A first analysis of the spectra obtained with the ultraviolet spectrometer SUMER is presented in a complementary paper (Innes, McKenzie, and Wang, 2003, hereinafter Paper I). It is demonstrated that, in the most part, the EUV darkness is caused by an absence of plasma (plasma void) not absorption of EUV emission by cold neutral material. The question of what the plasma voids are and how they are formed was avoided because there is still data, some of which will be described in this paper, to be analyzed.

Similar supra-arcade flare events have been seen in *Yohkoh*/SXT images (Švestka *et al.*, 1998; McKenzie and Hudson, 1999; McKenzie, 2000). All were associated with coronal mass ejection (CME). It was proposed by McKenzie and Hudson (1999) and McKenzie (2000) that the inflows are shrinking magnetic flux tubes that have been either stretched by the CME or disconnected from the CME at a reconnection site in the corona. Another possibility, suggested by Sheeley and Wang (2002), is that the supra-arcade inflows are smaller scale counterparts of coronal inflow events seen in white light LASCO images. They conclude that the

Solar Physics **217:** 267–279, 2003.

darkness is density depletion in the wake of infalling plasma. Further they suggest that bright loops form at the head of the inflow as a consequence of reconnection in the inflow. Both these reconnection scenarios would generate fast high-temperature plasma in the vicinity of the dark inflow.

The SUMER data, described in Paper I, confirm that the darkness is mostly due to an absence of plasma. On the other hand there is also some evidence for cold, high density material just in front of one of the main dark inflows. It is, therefore, appropriate to consider the structure around infalling plasma clouds. The 2D magnetohydrodynamic simulations of high-velocity clouds colliding with a magnetized galactic disk (Santillán *et al.*, 1999) look remarkably like the observed supra-arcade flows. But for such models to be relevant, the cloud velocity must be super-Alfvénic in order to compress the magnetic field in front and to create a cavity in its wake. This implies flow velocities greater than 450 km s^{-1} for a coronal magnetic field 5 G and density 10^9 cm^{-3}. It is roughly the same as the largest plane-of-sky speeds measured from X-ray images (McKenzie, 2000) so such models are a possibility. More applicable however may be simulations of two fluid plasma–plasma interaction as low-density plasma (e.g., the solar wind) flows past small, dense plasma clouds (Baumgärtel and Sauer, 1992; Sauer *et al.*, 1992). These show interesting effects that may be especially relevant to the sunward flows. Pressure gradients across the boundary of the two plasmas generate an electric field that acts on the wind like a Laval nozzel. A sub-Alfvénic wind is pushed apart and accelerated as it flows past the cloud. This generates a low-density cavity in the wake of the cloud with fast super-Alfvénic wind flow along its edge. Thus dense plasma clouds falling into the Sun with sub-Alfvénic speed would accelerate the ambient plasma to super-Alfvénic velocity.

Both high-velocity flows due to reconnection and wind acceleration past clouds could generate substantial Doppler shifts in SUMER lines. This paper discusses observations of high Doppler shifts in the Fe XXI line emitted by 10^7 K plasma. Some attempt will be made to identify the sites of the high-velocity flows but a thorough investigation of the interaction between the inflows and arcade dynamics is beyond the scope of this paper. The phase discussed starts about 30 min after flare onset. During this phase, the SUMER field of view coincided with the top of the supra-arcade structure. There was a rapid increase in Fe XXI emission as well as smaller-scale regions of C II brightening (Wang *et al.*, 2002). The period ends at the time of the strong sunward flows. After this time there are no more measurements of large Doppler shifts and the supra-arcade has risen beyond the position of the SUMER slit.

2. Observations and Data Analysis

A detailed description of the SUMER and TRACE 195 Å images is given in Paper I, together with an overview of the arcade evolution. The SUMER ultraviolet

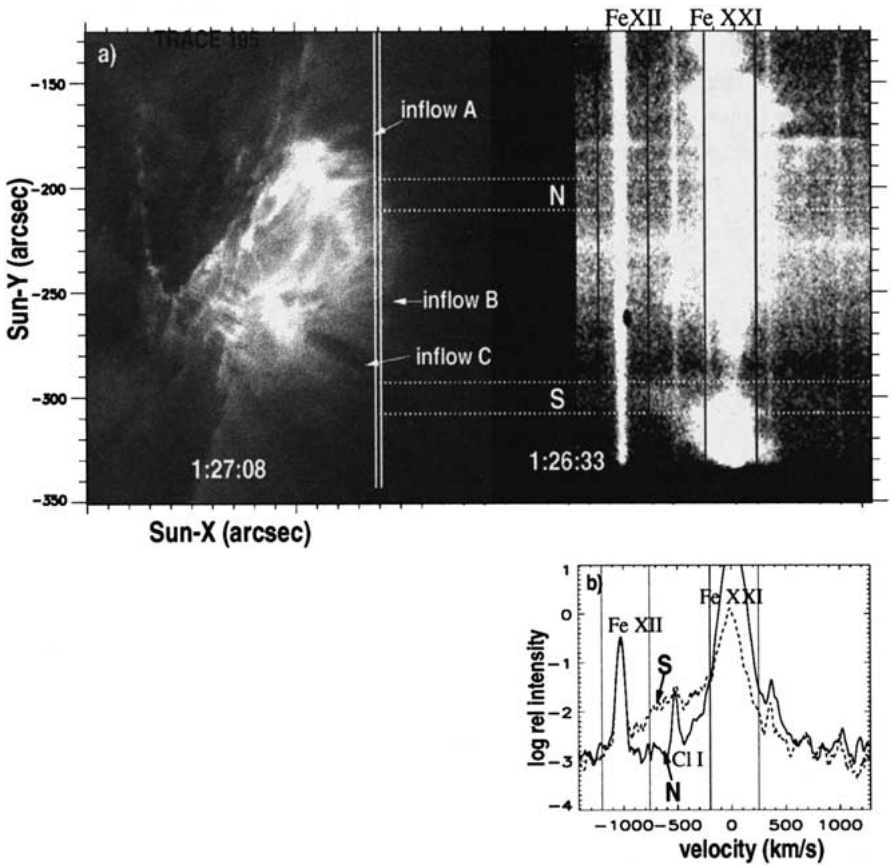

Figure 1. The TRACE 195 Å image and SUMER spectrum around region 1346.5–1360 Å, taken at the time when the top of the supra-arcade is in the SUMER field of view. Line spectra of the two regions marked with *dotted lines*, labeled 'N' and 'S' in the image, are compared in the plot below. Wavelength increases from left to right. The intensity of the weaker, *dashed line* spectrum from 'S', has been multiplied by a factor 10 so that the continua on the blue side (*left*) of Fe XII overlap. The position of the SUMER slit is marked as a *double vertical white line* on the TRACE image. The *vertical black lines* on the SUMER spectral image, and profiles delineate the edges of the data windows. The *black dot* near Sun-Y $= -260$ on the Fe XII line is a detector defect.

spectrometer obtained stigmatic images of the C II 1335 Å, Fe XII 1349 Å and Fe XXI 1354 Å lines at a fixed position of the flaring active-region corona. The discussion in this paper concentrates on spectra in the Fe XII and Fe XXI windows taken during the early phase of arcade growth, between 01:15 UT and 01:35 UT. The C II data have been discussed in Paper I.

3. Fe XXI Doppler Shifts

The narrow 2 Å spectral windows allow Doppler shift measurements ± 250 km s^{-1} around each line. This is usually sufficient to obtain line center shifts but not to detect the 1000 km s^{-1} shifts reported in this paper. As described here, these high-velocity shifts are Fe XXI shifts seen as an asymmetry in the continuum intensity around the Fe XII line which lies 4 Å or 1000 km s^{-1} to the blue of Fe XXI.

The spectral regions around the Fe XII to Fe XXI lines from the full detector spectrum taken at 1:26:33 UT are shown in Figure 1, alongside a contemporaneous TRACE image. The Fe XXI line is complex with broad and non-symmetric red and blue wings. As can be seen in this spectrum the 2 Å window is much too narrow to see the full width of the Fe XXI line.

The largest shift is a blue Fe XXI shift near Sun-Y $= -300$. It has emission out to the Fe XII line. The line profile from the region between dotted lines, marked 'S' (South) is shown as a dashed line in Figure 1(b). It is compared to the line profile from the region between the other pair of dotted lines in the image, marked 'N'. Region 'N' is chosen because it is the section along the slit with the most symmetric line profile and so highlights the large blue wing asymmetry at 'S'. Figure 1(b) clearly shows that the 'S' Fe XXI line extends out to the Fe XII line at -1000 km s^{-1}.

In the following analysis, I(red) is the average intensity in the five edge pixels on the red (right) side of the Fe XII window and I(blue) is the average of the five edge pixels on the blue (left). If only the windows had been transmitted at this time, the Fe XXI line shift from 'S' would have produced a factor 5 increase in I(red)/I(blue). Along the other parts of the slit, the differences in the continuum intensity at the red and blue edges of the Fe XII window are less than a factor 2. Thus although the Fe XXI window only goes to 250 km s^{-1}, it is possible to use the ratio I(red)/I(blue) in the Fe XII continuum intensity to identify Fe XXI blue shifts with velocity greater than 800 km s^{-1}.

Other possible contributions to an increase in I(red)/I(blue) are the two lines between the Fe XII and Fe XXI (Figure 1). The photospheric Cl I 1351.62 Å (-500 km s^{-1}) is scattered light from the solar disk and unlikely to produce large shifts. The other is the coronal Si IX 1353.42 Å and expected to have similar behavior to the Fe XII.

3.1. 1000 KM S^{-1} BLUE SHIFTS

The TRACE image in Figure 1 shows that the large Doppler shift at 'S' is from a position along the southern edge of a large dark inflow. The other positions of high shift in this spectrum, near Sun-Y $= -250$ and Sun-Y $= -160$, also seem to align with the boundary of a dark inflow. Thus it seems as if the highest shifts are coming from the edges of dark channels in the TRACE images. In this section time-space maps of the region observed by SUMER are investigated to see whether very

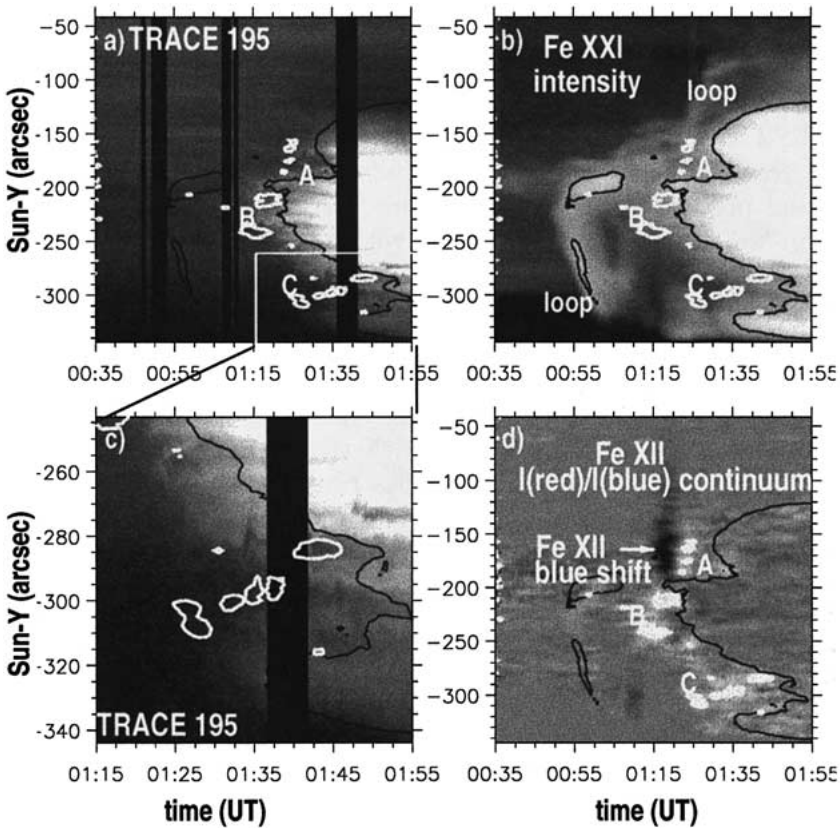

Figure 2. Time–space images showing the evolution of the TRACE 195 Å, Fe XXI and Fe XII line features in the corona at the position of the SUMER slit. (a) Log TRACE 195 Å intensity. The sunward flows show up as dark lanes in the supra-arcade emission. (b) Log of line-integrated Fe XXI intensity. (c) An expanded view of the time variation of the TRACE emission around the sunward flows in region 'C' (marked with a white box in (a)). (d) Log of the ratio of average intensity in the five pixels on the short (*left*) and long (*right*) wavelength edges of Fe XII window. *Black* shows where the short edge intensity is 3 times the long edge intensity (Fe XII blue shifts) and *white* shows where the long edge intensity is three times the short edge intensity (Fe XXI blue shifts or Fe XII red shifts). The *black contours* on all four figures outline brighter Fe XXI regions. The *white contours* outline the regions with greater than factor 3 more intensity on the long than the short wavelength edges of the Fe XII window.

high Fe XXI blue shifts or rather its proxy, $I(\text{red})/I(\text{blue})$ are seen at other times. In Figure 2, time–space maps of TRACE 195 Å and Fe XXI intensities are shown together with the variations of $I(\text{red})/I(\text{blue})$. Features of these maps have been described in Paper I, and the positions of prominent Fe XXI and Fe XII line shift features pointed out.

The focus now is the white areas in Figure 2 that are contoured in white on the other images. These regions have $I(\text{red})/I(\text{blue})$ greater than 3. On Figure 2, three regions have been labeled. Each of the regions shows dark inflows in Figure 1 and

sunward flows descending into bright arcade emission 5–10 min after a significant increase in the Fe XII I(red)/I(blue) continuum ratio.

Region 'A' is the region with the large Fe XXI red shift in the spectrum Figure 1(a). An example of the Fe XII and Fe XXI line profiles around this time and position are shown in Figures 3(c) and 3(d). Although there is asymmetry in the Fe XII continuum, the intensity is very weak. Additional support that there really is an Fe XXI blue shift is that the Fe XXI line in the Fe XXI window has a bright blue wing to at least -200 km s^{-1}.

The other two regions 'B' and 'C' have very convincing Fe XII continuum asymmetry. Examples of the spectra are shown in Figure 3. The Fe XII asymmetry around 'B' in Figure 3(a), is a strong feature and extends about 30 arc sec along the SUMER slit. The profile in Figure 3(a), shows about 4 times more counts on the long wavelength edge. The asymmetry from this region only lasts 2–3 min. At 01:24:48 UT, the continuum at this position is symmetric around the Fe XII line but is asymmetric about 30 arc sec further south (Figure 3(e)).

An example of SUMER spectra from region 'C', has been discussed (Figure 1). In this case, the red wing enhancement is without doubt due to 1000 km s^{-1} blue shifted Fe XXI. This high-velocity emission is already visible in the spectrum at 01:24:48 (Figure 3(g)). The enhancement of the red edge of the Fe XII window looks very similar to that seen in the full spectrum. It is also seen in all intervening images and is not related to the strength of the continuum or the strength of the Fe XXI or Fe XII line.

3.2. Relationship to supra-arcade dynamics

In Figure 2 it looks as though the high-velocity Fe XXI shifts appear 5–10 min before the sunward flows. This is true at the height of the SUMER slit because the sunward flows are only seen against the bright emission from the arcade. The 5–10 min time delay is the time needed after the blue-shift detection for the arcade to grow to the height of the SUMER slit position. The sunward flows are seen in TRACE images at lower heights from 01:10 UT onwards.

To identify the sunward flows in the TRACE images in a simple semi-automated way the images were rotated so that the limb, at the position of the flare, is parallel to the X-axis and regridded so that the supra-arcade rays are as far as possible perpendicular to the limb. Then running difference maps along narrow vertical sections of the regridded images were constructed. In these maps the upward and downward flows show up as features with positive and negative slopes. The regrid was defined by first adding all the images between 01:20 and 02:00 UT so that the average shape of the active region could be seen. Then a quadrilateral box was put around the main emission. This boxed region of the images was remapped onto a rectangular grid. Examples of the regridded images are shown in Figure 4. Due to the fanning out in the corona, the solar co-ordinates along the limb and corona (the X-axes in these images) are different. The Y-axis is the distance outwards

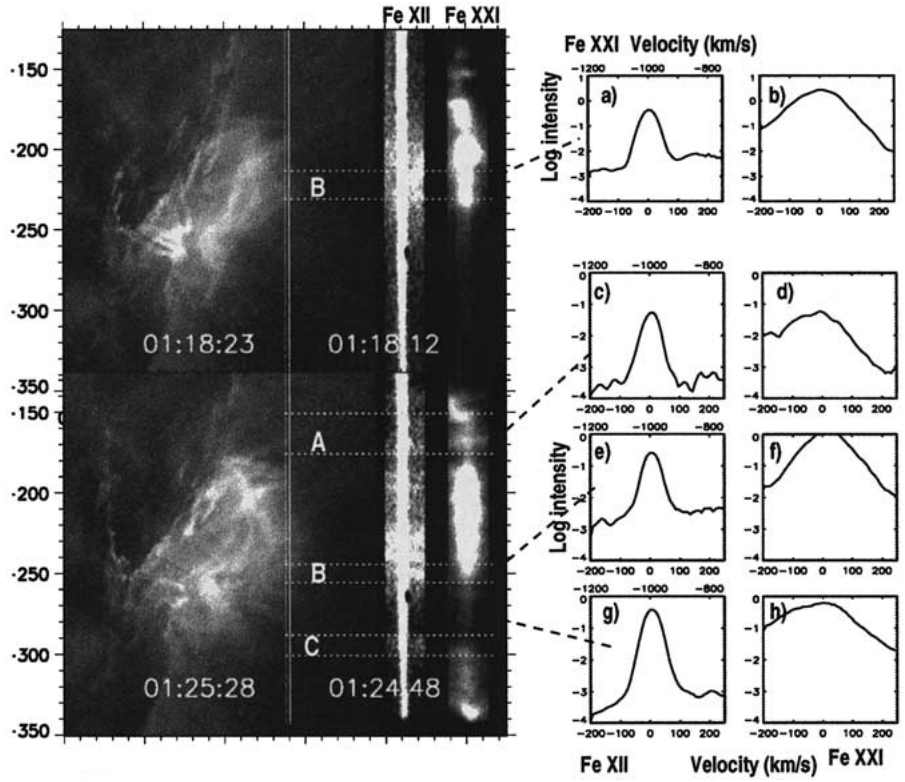

Figure 3. TRACE images and SUMER spectra at times of enhanced continuum on the long-wavelength side of the Fe XII window. The images on the left display SUMER Fe XII and Fe XXI data co-aligned to the TRACE image nearest in time. The profiles on the right are Fe XII and Fe XXI line profiles averaged over the sections between *dotted lines*. The Fe XII profiles (*left profiles*) have the Fe XII velocity shift on the bottom axis and the Fe XXI on the top. The enhancement ratios, I(red)/I(blue) of the Fe XII continuum, are from the top to the bottom of the figure (a) 3.5 from region 'B' (c) 2 from region 'A', (e) 4 from region 'B' and (g) 4 from region 'C'.

into the corona. Examples of time difference maps for vertical sections with width 5 arc sec and a 1 min time difference are shown in Figure 5. The Sun-Y position at the SUMER slit and, in brackets, the limb positions of the maps are given in black numbers at the top of each image. The section with distance -260 (-241) is shown in Figure 4.

With the help of the images in Figure 4 and Figure 2 the main features of these Figure 5 difference maps can be linked to disk and corona activity. The limb is around Dist. $= 25$ arc sec. On disk flaring produces the speckled white and black pattern below this Dist. The main flare arcade, which lies between 20 arc sec and 60 arc sec, is characterized by gradual downward directed bright and dark features with velocity around ~ 10 km s^{-1}. The bright and dark structure is probably due to loops with different temperature having emission in and out of the 195 Å filter window. At most positions, it can be seen that the brighter emission darkens as

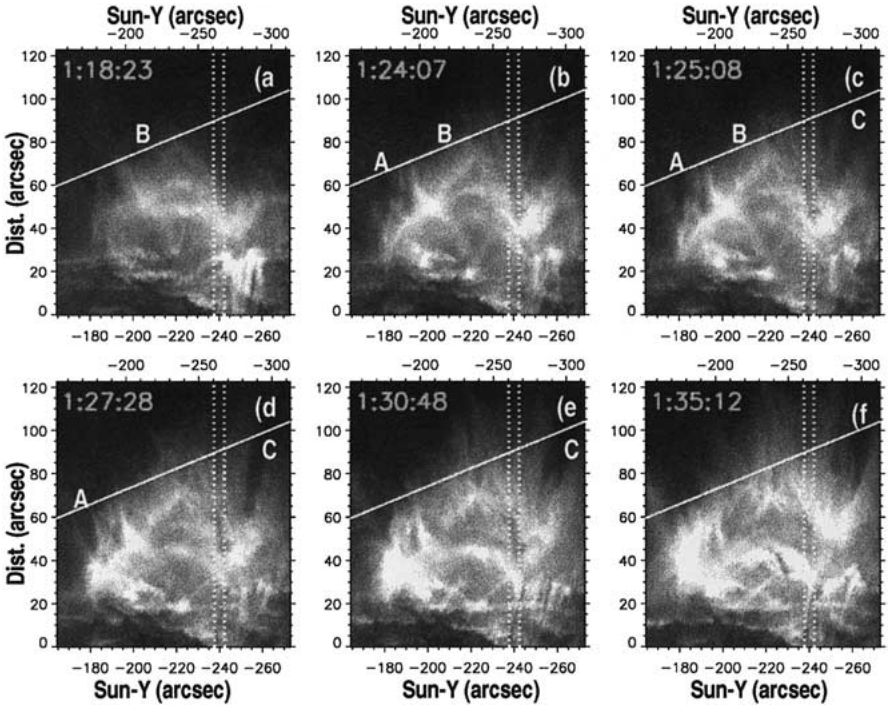

Figure 4. TRACE images of the supra-arcade regridded so the limb is parallel to the X-axis and the arcade rays are approximately vertical. The regridding shifts and compresses the corona with respect to the limb so that in these images the Sun-Y values along the top of the images are different from those along the bottom. The *solid white line* through the corona is the position of the SUMER slit. The *vertical dotted lines* delineate the section used to construct the running difference image Figure 5(g) at −260 (−241). The positions of the three regions A, B, and C discussed in the text are labeled.

it reaches the limb which is an indication that the EUV loops are cooling as they contract towards the limb (cf., Švestka *et al.*, 1987). Above about 60 arc sec is the activity of the supra-arcade. Here the dark downward flow is typically 40–60 km s^{-1}. The speed in the corona is probably much faster because there is usually a dark hook on the corona end of the inflows. The dark inflow in Figure 5(h) at 01:35 UT is seen exceptionally well in the corona. Its downward speed is about 400 km s^{-1}. Sometimes it looks as though the arcade top moves up soon after the downward flow breaks its speed near the top of the arcade. At distances −217 (−210) and −260 (−241) there are examples where this happens near the position of the SUMER slit.

These images give the impression that all the arcade top activity is coming from the corona. It may be exaggerated because the regrid was defined to track the corona rather than the disk activity. Thus jets from the disk that are directed along other angles show as brightenings for a short time rather than a complete track. One example is the disk flaring activity near limb position (−200) between

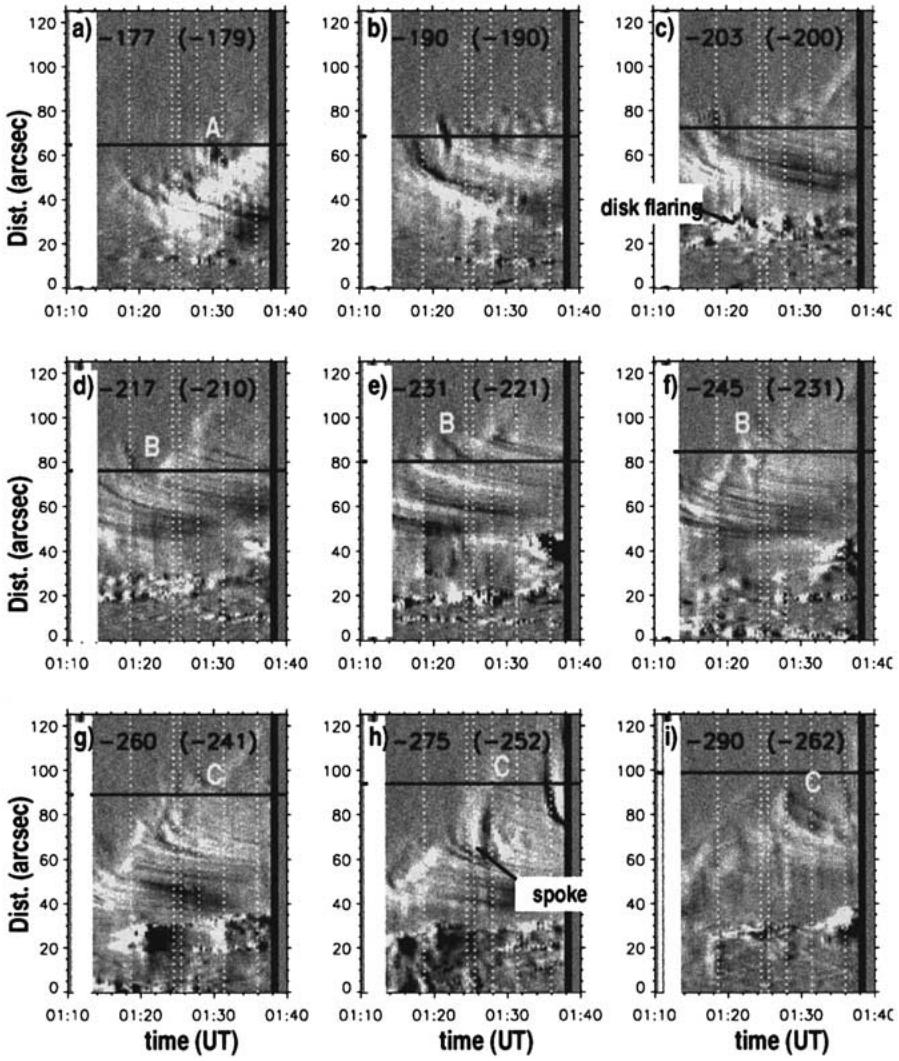

Figure 5. Time variations of TRACE intensity along vertical sections of the regridded images. The width of the vertical sections is 5 arc sec. A relative intensity increase (decrease) of 10% in 1 min is *white* (*black*). The Sun-Y co-ordinates at the height of the SUMER slit and, in brackets, the Sun-Y limb co-ordinates of the sections are given in black at the top of each image. The *solid black horizontal line* shows the SUMER slit position. The *dotted white lines* mark the times of the images in Figure 4. The times of the regions A, B, and C are marked on the figure at the appropriate position.

01:18 and 01:24 UT which shows up as a disk brightening with a vertical extension in Figure 5(c) at 01:21 UT. Steep slopes in the difference images are also created when spokes or dark channels swing in or out of the section during the time series. These are usually easy to identify by looking at the TRACE image sequence. An example is in Figure 5(h) at 01:25 UT.

Here we naively investigate links between corona down and up flow and the high Fe XXI blue shifts. We concentrate on the three regions marked A, B, and C on Figure 2. The first high blue shift (Figure 2(d), region 'B') is $-240 \leq$ Sun-Y ≤ -210 (-225 to -205) between 01:18 and 01:25 UT. The first image in Figure 4 is at time 01:18:23 UT. This time is marked with the first of the white vertical dashed lines on the maps in Figure 5. According to the running difference images, there is a sunward flow just crossing the SUMER slit at this time (Figure 5(d)). We have labeled it 'B'. It is also identified on Figure 4 as the broad dark cusp shaped feature near the center.

The high shifts in region 'A' start around 01:22 UT at Sun-Y$= -190$. They seem to be associated with the northern Fe XXI loop marked in Figure 2(b). Initially this region was dark in the TRACE images possibly because it was colder and only produced Fe XXI, not Fe XXIV emission. The TRACE intensity variations are shown in Figure 5(a). There is a TRACE brightening at the height of the SUMER slit at 01:27 UT (the fourth white dotted line). It seems to be due to a growing loop system and activity on the disk (Figure 4(d–f)). At 01:30 UT a downflow crosses the SUMER slit (Figure 5(a)), and SUMER registers a possible Fe XXI blue shift from 'A' (Figure 2(d)).

The third region is the most spectacular inflow region, marked 'C' on Figure 2. The region, around $-260 \geq$ Sun-Y ≥ -300, is covered by images Figures 5(g), 5(h), and 5(i). The high blue shifts are mostly seen from 01:24 UT until 01:28 UT. There is one strong inflow that starts at 01:27:28 (fourth white line) and seems to clear the supra-arcade of emission in the -290 (-262) section. It is actually a couple of inflows. Later the inflows merge and develop into the long narrow dark cusp structure seen in Figure 4(d). The almost vertical brightening and subsequent darkening in Figure 5(h) at 01:25 UT is caused by the boundary of this inflow swinging in and out of this particular vertical section.

4. Discussion

There is evidence from SUMER spectra of 1000 km s^{-1} Fe XXI plasma flow above the main flare arcade. Blue-shifted line emission is seen at the same time as inflows from the corona reach the arcade top. A sketch of the geometry is shown in Figure 6. The high Doppler shifts seem to be coming from the boundary along the tail of the dark inflows and the arcade. They are not associated with the main supra-arcade loops. Throughout most of the observing sequence only the blue wing of Fe XXI could be observed and it is not known whether there are equivalent high-velocity red shifts or not.

The Doppler-shift velocity is roughly the expected Alfvén velocity for a corona with magnetic field strength 10 G and density 10^9 cm^{-3}. It is slightly less than twice the free-fall speed and the observed plane-of-sky inflow speed. Such high velocities can, at first glance, be incorporated into reconnection models (McKenzie

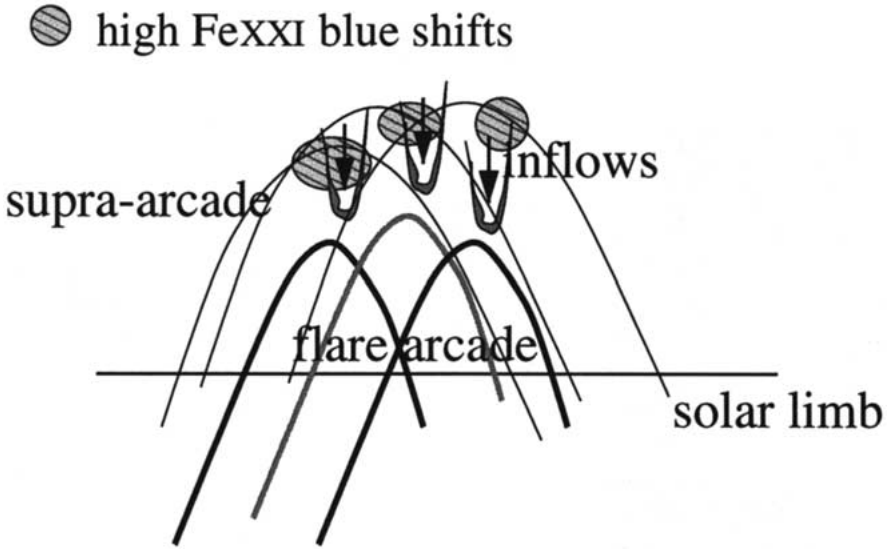

Figure 6. Sketch showing the position of high Fe XXI Doppler shifts and inflows in relation to the flare arcade and supra-arcade loops.

and Hudson, 1999; McKenzie, 2000; Sheeley and Wang, 2002) and solar wind acceleration past dense plasma clouds (Baumgärtel and Sauer, 1992; Sauer *et al.*, 1992). No model has been worked out in sufficient detail to really predict Doppler shifts, inflows and EUV intensities.

If the dark inflows are magnetic flux tubes disconnected at a reconnection site, then according to the models (Carmichael, 1964; Sturrock, 1968, Hirayama, 1974; Kopp and Pneuman, 1976; Yokoyama and Shibata, 2001) a fast, hot plasma jet would be behind the flux tube. At the head of the jet, there would be a fast magnetosonic shock and along the sides slow magnetosonic shocks. The 2D simulations by Shibata (2001) predict a bright reconnection jet and fast shock. The predicted intensity bares little resemblance to the supra-arcade spoke and inflow structure but then the real flows are 3D not 2D. The basic observation that the high-velocity Doppler flow is behind the disconnected plasmoids is predicted by this scenario. Likewise the reconnection scenario proposed by Sheeley and Wang (2002), in which reconnection is somehow triggered in the tail of the plasma void, would predict high Doppler shifts along the dark tail boundary.

Plasma acceleration past infalling dense clouds also predicts a fast wind behind dark inflows. This model, however, also predicts a long, low density tail behind the cloud. The observed oscillation (Figure 2(c)) could be explained as instability along the tail boundary. But there are many open questions. The most troubling is whether the combination of 400 km s^{-1} infall, magnetic field and slow outflowing active region wind is sufficient to generate 1000 km s^{-1} line-of-sight velocity without requiring a very special geometry. It is hoped that future calculations of

multi-fluid plasma interaction will be able to answer this question. Another nagging point is that SUMER did not detect absorbing material in the dark lanes (Paper I). Some absorption was detected, however, near position 'C', just before the arcade emission reached the height of the SUMER observations.

The third explanation is that the TRACE images are simply confusing the interpretation by showing an apparent link to the inflows and they have nothing to do with each other. RHESSI measured hard X-ray bursts (Gallagher *et al.*, 2002) at 01:15:44 and 01:23:19 UT, which is 2 min before the two main high Fe XXI Doppler-shift phases ('B' and 'C') were seen in the corona. The bursts appeared to come from loop footpoints on the disk so the Doppler shifts may simply be related to the disk hard X-rays. It is hoped that further analysis of the combined TRACE and SUMER data from this and, with some luck, future events will reveal the underlying physics.

Acknowledgements

These observations could not have been obtained without the help of the SUMER planners Cristian Vocks and Werner Curdt. Konrad Sauer proposed multi-fluid plasma interaction to explain the origin of the dark inflows and Jim McKenzie helped clarify some of the underlying physics. We would also like to thank Hugh Hudson for his encouraging comments. The SUMER project is financially supported by DARA, CNES, NASA and the ESA PRODEX programme (Swiss contribution). SUMER and MDI are part of SOHO, the Solar and Heliospheric Observatory of ESA and NASA.

References

Baumgärtel, K. and Sauer, K.: 1992, *Ann. Geophys.* **10**, 763.

Carmichael, H.: 1964, in W. N. Hess (ed.), *the Physics of Solar Flares*, NASA SP-50, NASA, Washington DC, p. 451.

Gallagher, P. T., Dennis, B. R., Krucker, S., Schwartz, R. A., and Tolbert, A. K.: 2002, *Solar Phys.* **210**, 341.

Hirayama, T.: 1974, *Solar Phys.* **34**, 323.

Innes, D. E., McKenzie, D. E., and Wang, T. J.: 2003, *Solar Phys.*, **217**, 247, Paper I.

Kopp, R. A. and Pneuman, G. W.: 1976, *Solar Phys.* **50**, 85.

McKenzie, D. E.: 2000, *Solar Phys.* **195**, 381.

McKenzie, D. E. and Hudson, H. S.: 1999, *Astrophys. J.* **519**, L93.

Santillán, A., Franco, J., Martos, M., and Kim, J.: 1999, *Astrophys. J.* **515**, 657.

Sauer, K., Roatsch, T., Baumgärtel, K., and McKenzie, J. F.: 1992, *Geophys. Res. Lett.* **19**, 645.

Sheeley, Jr., N. R. and Wang, Y. -M.: 2002, *Astrophys. J.* **579**, 874.

Sturrock, P. A.: 1968, in: K. O. Kiepenheuer (ed.), 'Structure and Development of Solar Active Regions', *IAU Symp.* **35**, 471.

Švestka, Z. F., Fontenla, J. M., Machado, M. E., Martin, S. F., and Neidig, D. F.: 1987, *Solar Phys.* **108**, 237.

Švestka, Z. F., Fárník, F., Hudson, H. S., and Hick, P.: 1998, *Solar Phys.* **182**, 179.
Wang, T. J., Solanki, S., Innes, D. E., and Curdt, W.: 2002, in H. Sawaya-Lacoste (ed.), 'Magnetic Coupling of the Solar Atmosphere', *IAU Colloq.* **188**, 607.
Yokoyama, T. and Shibata, K.: 2001, *Astrophys. J.* **549**, 1160.